



Right ventricular afterload in repaired D-TGA is associated with inefficient flow patterns, rather than stenosis alone

Marc Delaney¹ · Vincent Cleveland² · Paige Mass² · Francesco Capuano³ · Jason G. Mandell⁴ · Yue-Hin Loke⁴ · Laura Olivieri⁴

Received: 3 July 2021 / Accepted: 4 October 2021
© The Author(s), under exclusive licence to Springer Nature B.V. 2021

Abstract

Treatment of D-transposition of great arteries (DTGA) involves the Arterial Switch Operation (ASO), which can create PA branch stenosis (PABS) and alter PA blood flow energetics. This altered PA flow may contribute to elevated right ventricular (RV) afterload more significantly than stenosis alone. Our aim was to correlate RV afterload and PA flow characteristics using 4D flow cardiac magnetic resonance (CMR) imaging of a mock circulatory system (MCS) incorporating 3D printed replicas. CMR imaging and clinical characteristics were analyzed from 22 ASO patients (age 11.9 ± 8.7 years, 68% male). Segmentation was performed to create 3D printed PA replicas that were mounted in an MRI-compatible MCS. Pressure drop across the PA replica was recorded and 4D flow CMR acquisitions were analyzed for blood flow inefficiency (energy loss, vorticity). In post-ASO patients, there is no difference in RV mass ($p=0.07$), nor RV systolic pressure ($p=0.26$) in the presence or absence of PABS. 4D flow analysis of MCS shows energy loss is correlated to RV mass ($p=0.01$, $r=0.67$) and MCS pressure differential ($p=0.02$, $r=0.57$). Receiver operating characteristic curve shows energy loss detects elevated RV mass above 30 g/m^2 ($p=0.02$, AUC 0.88) while index of PA dimensions (Nakata) does not ($p=0.09$, AUC 0.79). PABS alone does not account for differences in RV mass or afterload in post-ASO patients. In MCS simulations, energy loss is correlated with both RV mass and PA pressure, and can moderately detect elevated RV mass. Inefficient PA flow may be an important predictor of RV afterload in this population.

Keywords Transposition of the great arteries (TGA) · 4D Flow · Cardiac Magnetic Resonance · Hemodynamics · Right ventricle · Afterload · Hypertrophy · Cardiac surgery · Stenosis

Introduction

D-transposition of the great arteries (DTGA) is a cyanotic form of congenital heart disease (CHD) that affects approximately 4.7 per 10,000 live births [1, 2] and invariably requires lifesaving surgical correction by way of the Jatene arterial switch operation (ASO) in the current surgical era

[3]. Long-term outcomes of increased survivorship and decreased reoperation rates have been observed since the ASO was widely adopted in the 1990s, in place of atrial switch operations (i.e. Mustard, Senning operations) [4, 5]. The oldest ASO patients are reaching young adulthood, and while long-term consequences of repair are not yet fully realized [6], current evidence indicates that these patients can develop significant mid-term hemodynamic complications [7]. In particular, hemodynamic changes after ASO can include right ventricular (RV) diastolic dysfunction, hypertrophy, and increased afterload [7–10]. Importantly, the pulmonary artery (PA) is heavily manipulated in the ASO through the LeCompte maneuver, where the pulmonary trunk and its bifurcation are translocated anterior to the neo-aorta [6]. This alteration of the PA morphology and how it affects the RV is a critical consideration to better understand the developing clinical picture of long-term complications.

✉ Marc Delaney
delaneyma@gmail.com

¹ Division of Pediatrics, Children's National Medical Center, 111 Michigan Ave, NW, Washington, DC 20010, USA

² Sheikh Zayed Institute for Pediatric Surgical Innovation, Children's National Medical Center, Washington, DC, USA

³ Department of Mechanics, Mathematics and Management, Politecnico di Bari, Bari, Italy

⁴ Division of Cardiology, Children's National Medical Center, Washington, DC, USA

The ASO manipulation of the pulmonary trunk and resulting altered PA morphology can introduce new PA bending, stretching, and stenosis [10–12]. Pulmonary artery branch stenosis (PABS) has received significant attention in the literature as a common and hemodynamically relevant complication, occurring in up to 60% of post-ASO patients [13]. PABS is thought to arise from both the anterior, stretched course of PA branches around the ascending aorta, and potentially compression from surrounding structures (i.e. sternum) [13–16]. While PA stenosis is an appealing etiologic factor to explain RV afterload in these patients, elevated RV mass and afterload are still observed in cases without apparent PA stenosis [9, 10].

Cardiac magnetic resonance imaging (CMR) has demonstrated that these variable PA morphologies lead to significant modification of PA flow patterns and hemodynamics [11, 14]. Flow irregularities observed in ASO patients include increased systolic flow velocity, asymmetric flow, and increased vortical flow dynamics compared to normal pulmonary vasculature [14]. Additionally, computational fluid dynamic (CFD) analysis using 3D mathematical modeling of post-ASO anatomy has further corroborated and elaborated on these flow anomalies, demonstrating increased presence of shear layer instabilities, vortical and helical flow patterns, and turbulent-like states [11, 17]. When flow becomes turbulent, the normally organized flow curve separates and forms secondary flow fields that create adverse pressure gradients and dissipate energy, causing flow inefficiency. This has been documented in bicuspid aortic valve and coarctation of the aorta [18, 19]. Importantly, in patients without apparent PA stenosis, abnormal PA flow patterns are still observed in this population [14] (see supplementary materials for further detail and formulae for energy loss, vorticity, and wall shear stress).

The goal of this study was to critically evaluate the role of PABS and PA flow patterns on RV afterload in repaired D-TGA patients using both clinical hemodynamic data and 4D flow imaging of a 3D printed replica within an in vitro mock circulatory system (MCS). Specifically, we hypothesized that RV afterload (defined by elevated RV mass and RV systolic pressure (RVSP)), would correlate with markers of PA flow inefficiencies from 4D flow (vorticity, energy loss), independent of pulmonary artery dimension.

Materials and methods

Patient selection and in vivo methods

Subjects and inclusion/exclusion criteria

This retrospective single-center study was approved by the Children's National Hospital Institutional Review Board.

Patients with D-TGA corrected via ASO with a clinically indicated CMR (including volumetry, 3D angiography and phase contrast imaging) and measurement of RV afterload (i.e. invasive pressure measurement or echocardiography estimate) within 6 months were reviewed for inclusion in this study. Subjects were excluded if there was evidence of pulmonary hypertension, previously placed pulmonary artery stent, or significant additional or residual heart disease was present (i.e. valve insufficiency, shunt, more than mild ventricular dysfunction, etc.). In subset analysis of this cohort for MCS simulations, patients were also excluded if the appropriate CMR sequences for volumetry analysis were unavailable. In the MCS experimental model, the physiologic pulsatile flow pump was unable to replicate flows that exceeded 300 mL/s. Thusly, patients whose MPA flow exceeded this value were also excluded from the in vitro experiments.

Clinical imaging data—echocardiography/catheterization

Measurements of RVSP were obtained within a 6-month period of the CMR study by either standard transthoracic echocardiography or invasive pressure measurement during cardiac catheterization. For transthoracic echocardiography, the RVSP was estimated by the tricuspid regurgitation jet gradient from continuous-wave Doppler added to the right atrial pressure (assumed to be 5 mmHg). When both echocardiogram and catheterization measurements were available, the catheterization measurement was utilized. Catheterization data predominated as the main source of RVSP measurements (50%, 11/22 patients) in this sample compared to echocardiography.

Clinical imaging data—CMR

All images were performed on a 1.5 T MR scanner (Aera; Siemens Healthcare, Erlangen, Germany) with an 18-channel body matrix array anteriorly. All sequence parameters, including repetition time (TR), echo time (TE), field-of-view (FOV), and voxel size, were performed in accordance with laboratory standards for cine, angiography, and flow sequences [20, 21]. Standard volumetry and right ventricular mass measurements were performed using MedisSuite (Medis, Leiden, Netherlands), with mass calculated as the volume of tissue between the epicardial and endocardial borders indexed to body surface area. Borders included trabeculations in the RV mass measurement, and standardized tissue density thresholds were used across the cohort. Vessel diameter in the MPA, RPA, and LPA were performed on 3D angiography datasets and referenced to obtain z-scores as previously reported in a healthy pediatric population by Knobel et al. [22]. PABS was defined as proximal right or left PA axial vessel diameter Z-scores less than negative two.

Flow measurements though the cardiac cycle were recorded in the MPA, RPA, and LPA from en face phase contrast images. Nakata index was chosen as a metric of PA size indexed to BSA, and was calculated as the sum of the cross-sectional area of the RPA and LPA divided by the body surface area (m^2) [23]. While the Nakata index was originally validated in Tetralogy of Fallot as well as Rastelli and Fontan patients, it has been shown to be consistent across infants and adolescents [23]. Nakata index was utilized here as an indexed continuous variable of PA size without the confounder of BSA to evaluate relationships between PA dimensions and hemodynamic variables, similar to previous studies [24, 25]. All measurements were performed by a blinded observer.

In vitro experimental model—the mock circulatory system

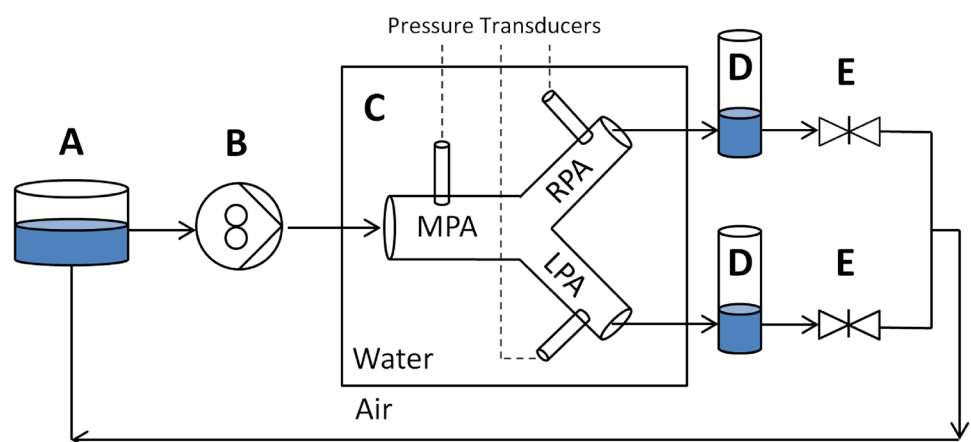
3D model creation

Segmentation was performed on contrast-enhanced MR angiograms to create models of the pulmonary artery bifurcation that were 3D printed and mounted in an MRI-compatible mock circulatory system (MCS). Segmentation was performed using standard techniques in commercial software (Materialise Mimics, Leuven, Belgium) and a 3D printable model was created (Materialise 3-matic, Leuven, Belgium) using our previously described lab standard [10, 11, 26, 27]. Models included the main pulmonary artery (MPA) origin to the first-order branch PA, with 5 mm extensions to gently transition to the uniform diameter and shape of circuit tubing. All models were 3D printed by stereolithography using a rigid polycarbonate-like material (Xometry, Gaithersburg, MD).

Mock circulatory system circuit layout and calibration

The models were submerged in water within a modular tank and connected in series to a closed circulatory circuit (Fig. 1) with major components including: MR-compatible pulsatile flow pump (CardioFlow 5000MR, Shelley Medical Imaging Technologies, ON, Canada), bilateral compliance-simulating chambers, and bilateral resistance-simulating adjustable valves. Flow parameters were recreated in a patient-specific manner, including flow over cardiac cycle, heart rate, and differential blood flow to right and left PAs. Two patients had in vivo 4D flow data, and this was used to validate the test bench model setup by comparison of in vivo and in vitro 4D flows. (see supplemental Fig. S1). Pressure transducers (Utah Medical Products, Midvale, UT) with data acquisition via LabView (National Instruments, Austin, TX) were utilized to calibrate system total resistance and collect pressure data. Maximum pressure differential (ΔP) across each model MPA to either branch PA (averaged over 10 cardiac cycles) was recorded as an analog of RV afterload. Iterative optimization of compliance model was performed using a two-element Windkessel model [28, 29]. After tuning the Windkessel, both in vivo and in vitro 4D flow data from a single patient geometry were compared (Figure #) with good agreement between average and unsteady flow conditions as validation. Given that not all patients had catheterization data, the overall resistance of the MCS circuit (set by pinch valves, Fig. 1E) was constant across the sample and optimized by iterative titration until the resultant pressure vs. time curves most closely matched the available kinetics and RVSP seen this cohort. Elements in the circuit were connected using semi-flexible tubing and a 40% glycerin-water (weight per volume) fluid mixture at room temperature was used to mimic blood viscosity [30, 31].

Fig. 1 Schematic of the Mock Circulatory System experimental setup. Included components of reservoir **A**, pulsatile and MR-compatible pump **B**, patient-specific PA model with pressure transducers contained within water tank **C**, compliance chambers **D**, and right and left lung resistance gate valves **E**



In vitro CMR and 4D data processing

A standard concentration of gadolinium contrast was added to this circuit and the flow pump setup was placed in a 1.5 T Siemens Aera scanner (Siemens Healthcare, Erlangen, Germany). Velocity encoding parameters were set based on in vivo PA velocity histogram and 4D flow sequences were acquired with the following settings: VENC 200–450 cm/s; echo time = 2.21 ms; repetition time = 38.16 ms; spatial resolution = 2.0 mm × 2.0 mm; slice thickness = 1.8 mm; flip angle = 15°; parallel acceleration factor = 2; number of phases = 30. Scanning time for 4D flow was approximately 7 min. 4D Flow sequences of each simulation were exported for offline analysis. Variables including peak systolic vorticity, energy loss during systole, and peak systolic wall shear stress were quantified (formulae available in supplementary materials) using ITFlow© software (Cardio Flow Design, Japan). Energy loss and vorticity are expressed as values and units normalized to segmented PA volume (mW/m³, and s⁻¹, respectively).

Statistical analyses

All statistical analyses were performed using GraphPad Prism version 8.4.3 for Windows (GraphPad Software, La Jolla, California USA). Comparisons of categorical variables performed with Fisher's exact test and comparisons of continuous variables were performed using paired or unpaired two-way t-tests. Correlations between continuous variables were assessed using Pearson correlation coefficient. Probability values < 0.05 were considered statistically significant.

Results

Demographics and clinical characteristics

22 patients (age = 11.9 ± 8.7 years, mean BSA = 1.2 ± 0.5 m², 68% male) were included in the clinical cohort analysis of RV afterload. Further investigation of this cohort with the MCS simulation was possible for 16 patients for pressure differential comparisons, and for 13 patients for RV mass comparisons after application of relevant exclusion criteria. Table 1 contains clinical characteristics of the cohort, including mean RV ejection fraction (58.7 ± 8.1%), mean right pulmonary blood distribution (53.5 ± 13.0%), mean RVSP of 38.4 (± 11.8) mmHg, and mean RV mass of 32.0 (± 10.5) g/m².

Full cohort analysis of RV afterload in the presence and absence of PABS

When dividing the clinical cohort by presence of PABS (proximal right or left PA axial vessel diameter Z-scores less than -2), we found that 64% of patients (14 of 22) had some form of PABS (unilateral or bilateral, Table 1). While 2 patients had bilateral stenosis, RPA stenosis was far more prevalent, as 50.0% of RPAs and 22.7% of the LPAs in the cohort were stenotic. Varying degrees of PABS were represented in this sample, with a mean Nakata index [23] of 163.33 (± 94.6) mm²/m² (reference range in original study population 330 ± 30 mm²/m²). *Flow measurements in the unilateral PABS cases demonstrated the average %RPA flow in the right-sided PABS group was 38.5% and 64.7%*

Table 1 Subject demographics, anatomy, and clinical characteristics

	Full Cohort	+ PABS	- PABS	P-Value
Demographics	<i>n</i> = 22	<i>n</i> = 14	<i>n</i> = 8	
Age (years)	11.9 (± 8.7)	14.7 (± 5.1)	10.7 (± 9.9)	0.387
Male Gender	68% (15/22)	64% (9/14)	75% (6/8)	0.999†
Body Surface Area (m ²)	1.2 (± 0.5)	1.1 (± 0.6)	1.4 (± 0.4)	0.164
Native Anatomy				
TGA, IVS*	68% (15/22)	71% (10/14)	63% (5/8)	0.999‡
Clinical Characteristics				
RV Systolic Pressure (mmHg)	38.4 (± 11.8)	40.6 (± 13.1)	34.5 (± 7.3)	0.259
RV Mass (g/m ²)	32.0 (± 10.5)	28.2 (± 10.8)	37.47 (± 6.9)	0.066
RV Ejection fraction	58.7% (± 6.5)	58.0% (± 5.6)	59.0 (± 7.5)	0.851
PA Flow Distribution (% RPA Flow)	53.5% (± 13.0)	51.7% (± 15.0)	56.7% (± 7.4)	0.409
Nakata Index (mm ² /m ²)	182.2 (± 96)	168.2 (± 109.2)	206.8 (± 59.6)	0.389

Values among subjects with and without pulmonary arterial branch stenosis (PABS), represented as mean ± standard deviation, with p-values provided

*Native anatomy of all other participants was TGA with ventricular septal defect

†Odds ratio 95% confidence interval: 0.1–3.5

‡Odds ratio 95% confidence interval: 0.6–2.8

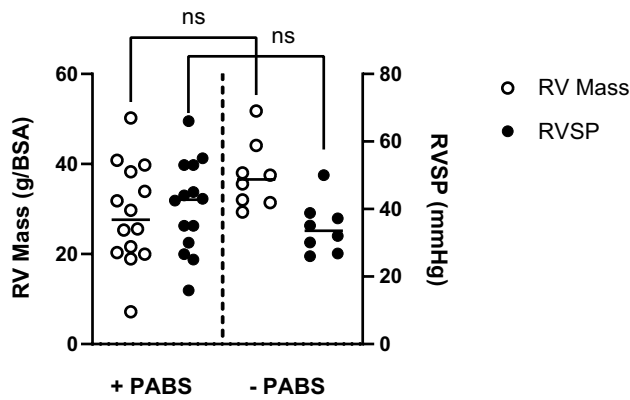


Fig. 2 Clinical measurements of RV failure are similar across PAs with and without stenosis. In the presence or absence of pulmonary arterial branch stenosis (\pm PABS, as defined by proximal axial PA diameter z-score less than -2) there is no difference in the mean RV mass (left axis, $p=0.066$), nor mean composite RVSP (right axis, $p=0.259$)

in the unilateral left PABS group. When comparing metrics of RV afterload in these subgroups, there was no difference in indexed RV mass ($p=0.066$) nor composite RVSP ($p=0.259$) between the PABS+ and PABS- groups (Fig. 2).

Cohort subanalysis of PA flow patterns using MCS simulations

RV mass measurements directly correlated with in vitro measurement of maximum systolic energy loss (mW/m^3) from the MCS ($p=0.012$, $r=0.67$, Fig. 3A). Similarly, RV mass significantly correlated with maximum systolic vorticity (s^{-1}) ($p=0.012$, $r=0.67$, Fig. 3B). Finally, RV mass showed no correlation with presence of pulmonary artery stenosis, as measured by the Nakata index ($p=0.071$, $r=0.52$, Fig. 3C).

Benchtop ΔP measurements from the MCS were significantly correlated to maximum systolic energy loss ($p=0.021$, $r=0.57$, Fig. 4A) and maximum wall shear stress ($p<0.001$, $r=0.85$, Fig. 4B), demonstrating a direct relationship between pressure drop over the right ventricular outflow tract and flow inefficiency. There was

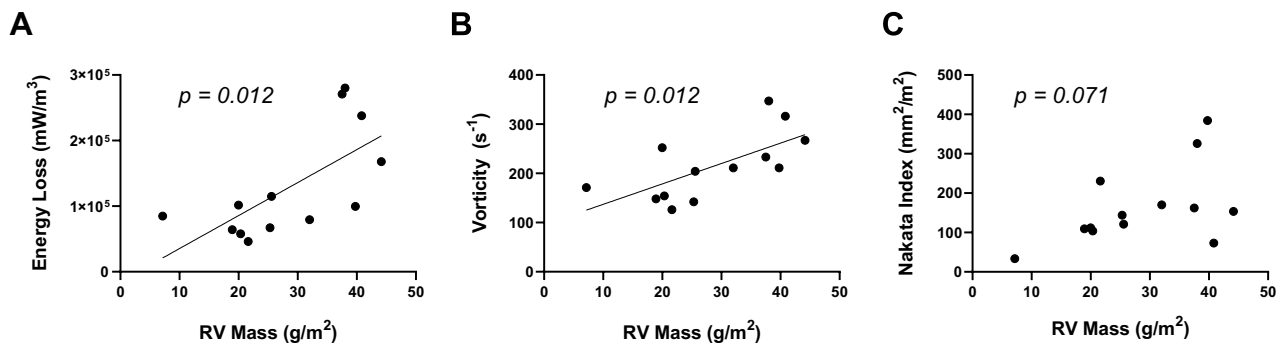


Fig. 3 RV mass is correlated to 4D Flow-derived metrics of flow inefficiencies, but not to stenotic index in the post-ASO pulmonary artery. Maximum systolic energy loss **A** and maximum vorticity **B** are

significantly correlated to indexed RV mass ($p=0.012$, $r=0.67$ and $p=0.012$, $r=0.67$, respectively). Nakata index is not correlated with RV mass (**C**, $p=0.071$, $r=0.52$)

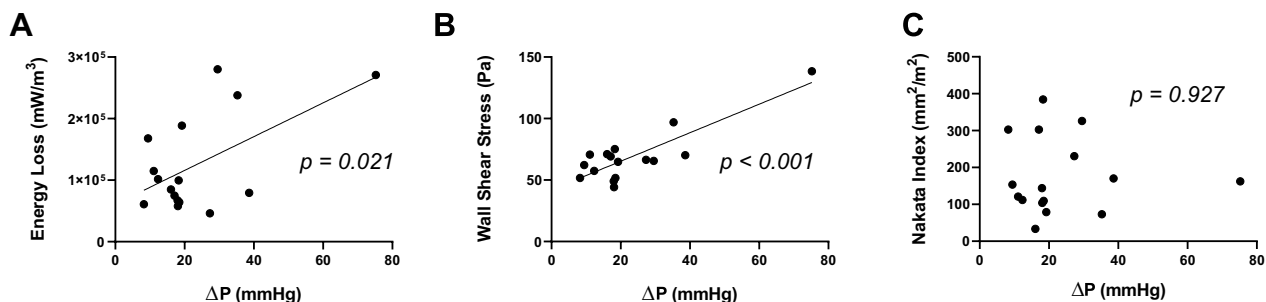


Fig. 4 MCS pressure differential is correlated to 4D Flow-derived metrics of flow inefficiencies, but not to stenotic index. Maximum systolic energy loss **A** and maximum wall shear stress **B** are sig-

nificantly correlated to pressure differential (ΔP) in the MCS circuit ($p=0.021$, $r=0.57$ and $p<0.001$, $r=0.85$, respectively). There is no correlation between ΔP and Nakata index (**C**, $p=0.927$, $r=-0.03$)

no correlation between ΔP and Nakata index (Fig. 4C, $p=0.927$, $r=-0.03$), indicating that pulmonary artery stenosis is not singularly responsible for these flow inefficiencies. Of note, ΔP was also shown not to be statistically significantly correlated with RV mass in this cohort ($p=0.408$, $r=0.43$).

Given the persistent association of energy loss to both RV mass and MCS pressure differential, we next sought to investigate if energy loss could predict the variation in RV mass better than stenosis alone via receiver operating characteristics (ROC) analysis. This demonstrated that maximum systolic vorticity from the branch pulmonary arteries, but not Nakata index, moderately detected the presence of elevated RV Mass ($> 30 \text{ g/m}^2$) ($p=0.022$, AUC 0.88; and $p=0.087$, AUC 0.79; respectively, Fig. 5C). There was no significant correlation between maximum systolic energy loss and left or right PA proximal axial diameter Z-score ($p=0.076$, $r=0.46$ and $p=0.965$, $r=-0.01$, respectively, Fig. 5D).

Discussion

Our study highlights the correlation between RV afterload and inefficient PA flow patterns that is not explained by presence of pulmonary artery stenosis in patients who have undergone the ASO. These data reveal that in a clinical cohort analysis, stenosis alone does not account for differences in RV mass or afterload in post-ASO patients. When further investigated in an MCS simulation, energy loss from inefficient flow is correlated with both increased RV mass and increased PA pressure and can moderately detect patients with elevated RV mass while PA dimension index alone cannot. This study reinforces earlier work regarding the importance of flow inefficiencies in post-ASO PA morphology and their impact on the development of RV failure [10, 11, 14].

Right ventricular hypertrophy is an important clinical endpoint to follow in the lifelong management of TGA

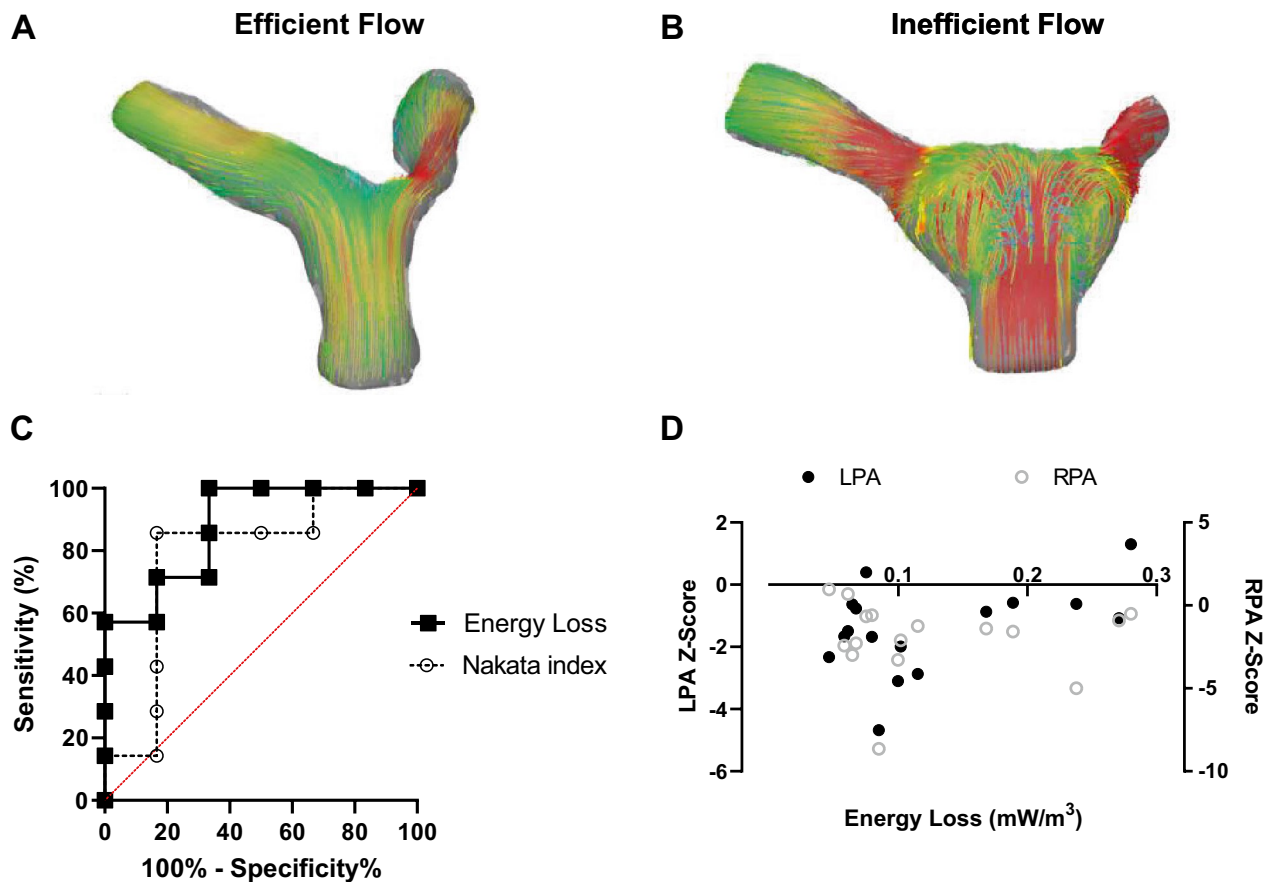


Fig. 5 Energy loss is not correlated with branch PA stenosis and offers improved detection of RV mass over stenotic index alone. Segmented PA models with streamlines are shown at peak systole, demonstrating relatively efficient flow patterns **A** compared with relatively inefficient flow patterns **B**. **C** Receiver operating characteristic curve shows that maximum systolic energy loss detects elevated RV

Mass above 30 g/m^2 ($p=0.022$, AUC 0.88) but Nakata index does not ($p=0.087$, AUC 0.79). **D** Maximum systolic energy loss and left (left axis) and right (right axis) PA proximal axial diameter Z-score exhibit no significant correlation ($p=0.076$, $r=0.46$ and $p=0.965$, $r=-0.01$, respectively)

patients, but its etiology remains poorly understood [8–10, 32]. Evidence from the context of pulmonary hypertension has enhanced the understanding of the RV maladaptive response to afterload [33]. In pulmonary hypertension pathophysiology, strain can lead to deficits in RV regional contractility and RV systolic and diastolic dysfunction, which have also been previously reported in TGA patients [8, 34, 35]. It's possible that circumferential RV strain patterns that are seen post-ASO may be an important precursor to RV hypertrophy [34].

The complex story of the etiology of RV hypertrophy in this context may also involve factors of proximal PA distensibility and coronary insufficiency. Evidence from CMR imaging of repaired aortic coarctation showed aortic stiffness was associated with increased LV Mass [36]. This relationship may apply to the RV as well, as retrospective cohort analysis in healthy adults has demonstrated an association between PA stiffness and RV hypertrophy and dysfunction [36, 37]. In the post-ASO heart, early work has suggested that PA stiffness is prevalent and this may be an important factor contributing to RV hypertrophy in these patients [38, 39]. Additionally, coronary abnormalities are frequent complications that may go unnoticed post-ASO and are thusly difficult to study [8]. Ischemic damage secondary to coronary insufficiency remains an additional contributing factor to the adaptive response of the RV and the development of RV hypertrophy after ASO [9, 40].

The contribution of 4D flow CMR technology to the understanding of congenital heart disease hemodynamics has drawn attention to the significance of flow disturbances in this context. Four dimensional flow technology has brought improved spatial and temporal encoding of CMR acquisitions, allowing for observation of vortical and helical patterns in the vessels of healthy control subjects as well as pathological study subjects [11, 41, 42]. The flow in normal PAs has been found to be smooth and highly hemodynamically efficient [43], supposedly as a result of the optimal curvature of the pulmonary bifurcation and uniform velocity profiles at the MPA inlet. In contrast, many authors have supported the observation of a greater degree of inefficient flow profiles in the pulmonary trunk of post-ASO patients [11, 14, 44]. From a mechanistic standpoint, flow inefficiencies (here quantified via energy loss) significantly contribute to increased RV systolic mechanical work, especially in the low-pressure biomechanical environment of the pulmonary circuit. This study adds to this understanding and provides an important clinical correlate of RV mass. Future work that continues to assess how flow patterns relate to clinical endpoints is warranted for furthering our understanding and clinical management of congenital heart disease.

Our study adds to a growing body of work aimed at understanding the broader effects of PA morphology on fluid mechanics and hemodynamics and is important to the

context of optimization of the surgical strategy in TGA. An example of variation in surgical strategy for TGA involves the spiral technique, aimed at emulating the normal spiral relationship that the great vessels have in healthy subjects [14, 17, 45]. In this surgical variation, CMR evaluation has shown the spiral technique to be associated with less helical flow and less vortex formation compared with LeCompte [45]. Similarly, computational fluid dynamics modeling indicates this arrangement to be associated with more homogeneous distribution of wall shear stress and outflow velocity in the RVOT [17]. Even in patients with ASO and LeCompte maneuver, analysis of pulmonary trunk position relative to the aorta in D-TGA patients showed that an anterior position was associated with increased MPA flow velocity, asymmetric flow, and increased vortical flow. While the LeCompte maneuver remains standard of care [46], these studies highlight the need for continued attention to these morphological differences as we learn more about the associated clinical outcomes.

Our study had several limitations. The single-center and retrospective nature, along with relatively limited sample size, limit the external validity of results. Exclusion of patients with previous PA stents and significant RVOT obstruction misses a subset of post-ASO patients, as these are relatively common mid-late term complications post-ASO [3, 47]. In addition, study participants most often underwent CMR and hemodynamic evaluation due to clinical concern for PABS, potentially introducing a bias in our sample that over-samples these more extreme PA geometries compared to the full post-ASO population. Additionally, our study did not examine velocity profiles of blood flow in the PAs in the evaluation of stenosis and focused on PA dimensions only. Clinical measurements of RVSP can be limited by acoustic windows and incomplete tricuspid regurgitation jets (echo) and by sedated/anesthetized loading conditions altering preload and afterload (cath). Other important limitations to this study arise from technical assumptions made in the MCS methodology. Our PA models were printed using a rigid material similarly to previously reported [48–50] whereas more recent MCS studies are investigating incorporating elastic models [28, 49, 51]. Rigid models offer advantages such as technical feasibility and standardization of vessel elasticity and compliance and comparison with computational fluid dynamics simulations that use rigid wall assumptions [48, 49]. However, variation in PA stiffness is observed post-ASO and elastic models incorporate the element of proximal vessel compliance into the MCS simulation, an element that could be reproduced even in a patient-specific manner [48, 49].

Our study is among the first of a growing body of literature that associates 4D flow-derived variables of fluid mechanics with clinically relevant factors in congenital heart disease. We found that RV afterload was associated with

inefficient PA flow patterns independently of PA dimensions alone. With further research, markers of flow inefficiency from 4D flow CMR may prove to be a clinically useful predictive tool for the management of complications and optimization of surgery in this growing patient population.

Supplementary Information The online version contains supplementary material available at <https://doi.org/10.1007/s10554-021-02436-4>.

Acknowledgements The authors would like to acknowledge Nicholas Mouzakis, the cardiovascular magnetic resonance technologist for assistance in scanning in vitro experiments.

Authors' contributions VC and PM made substantial contributions to experiment execution and engineering iterative design. FC provided technical oversight and guidance in optimizing patient-specific parameters of experimental setup. YL, JM, and LO provided scientific guidance and cardiology imaging expertise throughout and directly contributed to the study conception and execution. LO also served as the primary mentor and principal investigator for this research and contributed significantly to manuscript editing. All authors read and approved the final manuscript.

Funding This project was supported by Award Number R38AI140298 from the NIH National Center of Allergy and Infectious Diseases. Its contents are solely the responsibility of the authors and do not necessarily represent the official views of the National Center of Allergy and Infectious Diseases or the National Institutes of Health.

Data availability The datasets generated and analyzed during the current study are not publicly available in order to protect subject anonymity, but are available from the corresponding author on reasonable request.

Declarations

Conflict of interest The authors declare that they have no conflicts of interests.

Ethical approval This study was approved by the Children's National Hospital Institutional Review Board.

Consent for publication Not applicable, as no individual-level data has been presented in this manuscript.

Consent for publication Not applicable, as no individual-level data has been presented in this manuscript.

References

1. Reller MD, Strickland MJ, Riehle-Colarusso T, Mahle WT, Correa A (2008) Prevalence of congenital heart defects in metropolitan Atlanta, 1998–2005. *J Pediatr* 153:807–813
2. Gerberding J, Snider D, Popović T, Solomon S (2006) Improved national prevalence estimates for 18 selected major birth defects—United States, 1999–2001. *MMWR Morb Mortal Wkly Rep* 54:1301–5
3. Hutter P, Kreb D, Mantel S, Hitchcock J, Meijboom E, Bennink G (2002) Twenty-five years' experience with the arterial switch operation. *J Thorac Cardiovasc Surg* 124:790–797
4. Hörer J, Schreiber C, Cleuziou J, Vogt M, Prodan Z, Busch R, Holper K, Lange R (2009) Improvement in long-term survival after hospital discharge but not in freedom from reoperation after the change from atrial to arterial switch for transposition of the great arteries. *J Thorac Cardiovasc Surg* 137:347–354
5. Prêtre R, Tamisier D, Bonhoeffer P, Mauriat P, Pouard P, Sidi D, Vouhé P (2001) Results of the arterial switch operation in neonates with transposed great arteries. *The Lancet* 357:1826–1830
6. Jatene A, Fontes VF, Paulista P, Souza L, Neger F, Galantier M, Sousa J (1976) Anatomic correction of transposition of the great vessels. *J Thorac Cardiovasc Surg* 72:364–370
7. Kirzner J, Pirmohamed A, Ginns J, Singh HS (2018) Long-term management of the arterial switch patient. *Curr Cardiol Rep* 20:68
8. Klitsie LM, Roest AA, Kuipers IM, Hazekamp MG, Blom NA, Ten Harkel AD (2014) Left and right ventricular performance after arterial switch operation. *J Thorac Cardiovasc Surg* 147:1561–1567
9. Grotenhuis HB, Kroft LJ, van Elderen SG, Westenberg JJ, Doornbos J, Hazekamp MG, Vliegen HW, Ottenkamp J, de Roos A (2007) Right ventricular hypertrophy and diastolic dysfunction in arterial switch patients without pulmonary artery stenosis. *Heart* 93:1604–1608
10. Loke Y-H, Capuano F, Mandell J, Cross RR, Cronin I, Mass P, Balaras E, Olivieri LJ (2019) Abnormal pulmonary artery bending correlates with increased right ventricular afterload following the arterial switch operation. *World J Pediatr Congenit Heart Surg* 10:572–581
11. Capuano F, Loke Y-H, Cronin I, Olivieri LJ, Balaras E (2019) Computational study of pulmonary flow patterns after repair of transposition of great arteries. *J Biomechan Eng* 141:051008
12. Morgan CT, Mertens L, Grotenhuis H, Yoo SJ, Seed M, Grosse-Wortmann L (2017) Understanding the mechanism for branch pulmonary artery stenosis after the arterial switch operation for transposition of the great arteries. *Eur Heart J Cardiovasc Imaging* 18:180–185
13. Khairy P, Clair M, Fernandes SM, Blume ED, Powell AJ, Newburger JW, Landzberg MJ, Mayer JE (2013) Cardiovascular outcomes after the arterial switch operation for D-transposition of the great arteries. *Circulation* 127:331–339
14. Geiger J, Hirtler D, Bürk J, Stiller B, Arnold R, Jung B, Langer M, Markl M (2014) Postoperative pulmonary and aortic 3D haemodynamics in patients after repair of transposition of the great arteries. *Eur Radiol* 24:200–208
15. Ntsinjana HN, Capelli C, Biglino G, Cook AC, Tann O, Derrick G, Taylor AM, Schievano S (2014) 3D morphometric analysis of the arterial switch operation using in vivo MRI data. *Clin Anat* 27:1212–1222
16. Breinholt JP, John S (2019) Management of the adult with arterial switch. *Methodist DeBakey Cardiovasc J* 15:133
17. Tang T, Chiu S, Chen H-C, Cheng K-Y, Chen S-J (2001) Comparison of pulmonary arterial flow phenomena in spiral and Lecompte models by computational fluid dynamics. *J Thorac Cardiovasc Surg* 122:529–534
18. Yan W, Li J, Wang W, Wei L, Wang S (2021) A fluid-structure interaction study of different bicuspid aortic valve phenotypes throughout the cardiac cycle. *Front Physiol* 12:716015
19. Olivieri LJ, de Zélicourt DA, Haggerty CM, Ratnayaka K, Cross RR, Yoganathan AP (2011) Hemodynamic modeling of surgically repaired coarctation of the aorta. *Cardiovasc Eng Technol* 2:288–295
20. Fratz S, Chung T, Greil GF, Samyn MM, Taylor AM, Valsangiacomo Buechel ER, Yoo SJ, Powell AJ (2013) Guidelines and protocols for cardiovascular magnetic resonance in children and adults with congenital heart disease: SCMR expert consensus group on congenital heart disease. *J Cardiovasc Magnetic Reson* 15:51

21. Olivieri LJ, Jiang J, Hamann K, Loke YH, Campbell-Washburn A, Xue H, McCarter R, Cross R (2020) Normal right and left ventricular volumes prospectively obtained from cardiovascular magnetic resonance in awake, healthy, 0–12 year old children. *J Cardiovasc Magnetic Reson* 22:11
22. Knobel Z, Kellenberger CJ, Kaiser T, Albisetti M, Bergsträsser E, Buechel ER (2011) Geometry and dimensions of the pulmonary artery bifurcation in children and adolescents: assessment in vivo by contrast-enhanced MR-angiography. *Int J Cardiovasc Imaging* 27:385–396
23. Nakata S, Imai Y, Takanashi Y, Kurosawa H, Tezuka K, Nakazawa M, Ando M, Takao A (1984) A new method for the quantitative standardization of cross-sectional areas of the pulmonary arteries in congenital heart diseases with decreased pulmonary blood flow. *J Thorac Cardiovasc Surg* 88:610–619
24. Karaca-Altintas Y, Laux D, Gouton M, Bensemlali M, Roussin R, Hörer J, Raisky O, Bonnet D (2020) Nakata index above 1500 mm²/m² predicts death in absent pulmonary valve syndrome. *Eur J Cardio-Thoracic Surg* 57:46–53
25. Sandoval JP, Chaturvedi RR, Benson L, Morgan G, Van Arsdell G, Honjo O, Caldarone C, Lee KJ (2016) Right ventricular outflow tract stenting in tetralogy of fallot infants with risk factors for early primary repair. *Circ Cardiovasc Interv*. <https://doi.org/10.1161/CIRCINTERVENTIONS.116.003979>
26. Yeung E, Inoue T, Matsushita H, Opfermann J, Mass P, Aslan S, Johnson J, Nelson K, Kim B, Olivieri L, Krieger A, Hibino N (2020) In vivo implantation of 3-dimensional printed customized branched tissue engineered vascular graft in a porcine model. *J Thorac Cardiovasc Surg* 159:1971–1981.e1
27. Mandell JG, Loke YH, Mass PN, Opfermann J, Cleveland V, Aslan S, Hibino N, Krieger A, Olivieri LJ (2020) Aorta size mismatch predicts decreased exercise capacity in patients with successfully repaired coarctation of the aorta. *J Thorac Cardiovasc Surg*. <https://doi.org/10.1016/j.jtcvs.2020.09.103>
28. Knoops PG, Biglino G, Hughes AD, Parker KH, Xu L, Schievano S, Torii R (2017) A mock circulatory system incorporating a compliant 3d-printed anatomical model to investigate pulmonary hemodynamics. *Artif Organs* 41:637–646
29. Zambrano BA, McLean NA, Zhao X, Tan JL, Zhong L, Figueroa CA, Lee LC, Baek S (2018) Image-based computational assessment of vascular wall mechanics and hemodynamics in pulmonary arterial hypertension patients. *J Biomech* 68:84–92
30. Canstein C, Cachot P, Faust A, Stalder A, Bock J, Frydrychowicz A, Küffer J, Hennig J, Markl M (2008) 3D MR flow analysis in realistic rapid-prototyping model systems of the thoracic aorta: comparison with in vivo data and computational fluid dynamics in identical vessel geometries. *Magn Reson Med* 59:535–546
31. Biglino G, Giardini A, Baker C, Figliola RS, Hsia T-Y, Taylor AM, Schievano S (2012) In vitro study of the Norwood palliation: a patient-specific mock circulatory system. *ASAIO J* 58:25–31
32. Nyns EC, Dragulescu A, Yoo SJ, Grosse-Wortmann L (2016) Evaluation of knowledge-based reconstruction for magnetic resonance volumetry of the right ventricle after arterial switch operation for dextro-transposition of the great arteries. *Int J Cardiovasc Imaging* 32:1415–1423
33. Vonk-Noordegraaf A, Haddad F, Chin KM, Forfia PR, Kawut SM, Lumens J, Naeije R, Newman J, Oudiz RJ, Provencher S, Torbicki A, Voelkel NF, Hassoun PM (2013) Right heart adaptation to pulmonary arterial hypertension: physiology and pathobiology. *J Am Coll Cardiol* 62:D22–33
34. Thattaliyath BD, Forsha DE, Stewart C, Barker PC, Campbell MJ (2015) Evaluation of right ventricular myocardial mechanics using velocity vector imaging of cardiac MRI cine images in transposition of the great arteries following atrial and arterial switch operations. *Congenit Heart Dis* 10:371–379
35. Sanz J, Sánchez-Quintana D, Bossone E, Bogaard HJ, Naeije R (2019) Anatomy, function, and dysfunction of the right ventricle: JACC state-of-the-art review. *J Am Coll Cardiol* 73:1463–1482
36. Ou P, Celermajer DS, Jolivet O, Buyens F, Herment A, Sidi D, Bonnet D, Mousseaux E (2008) Increased central aortic stiffness and left ventricular mass in normotensive young subjects after successful coarctation repair. *Am Heart J* 155:187–193
37. Dawes TJ, Gandhi A, de Marvao A, Buzaco R, Tokarczuk P, Quinlan M, Durighel G, Diamond T, Monje Garcia L, de Cesare A, Cook SA, O'Regan DP (2016) Pulmonary artery stiffness is independently associated with right ventricular mass and function: a cardiac MR imaging study. *Radiology* 280:398–404
38. Aziz KU, Nanton MA, Kidd L, Moes CA, Rowe RD (1976) Variation in the size and distensibility of the pulmonary arteries in d-transposition of the great arteries. *Am J Cardiol* 38:452–457
39. Murakami T, Nakanishi T, Nakazawa M, Momma K, Imai Y (1998) The spectrum of pulmonary input impedance in children with complete transposition after the arterial switch operation. *Cardiol Young* 8:180–186
40. Yu CM, Sanderson JE, Chan S, Yeung L, Hung YT, Woo KS (1996) Right ventricular diastolic dysfunction in heart failure. *Circulation* 93:1509–1514
41. Liu X, Sun A, Fan Y, Deng X (2015) Physiological significance of helical flow in the arterial system and its potential clinical applications. *Ann Biomed Eng* 43:3–15
42. Bächler P, Pinochet N, Sotelo J, Crelier G, Irarrazaval P, Tejos C, Uribe S (2013) Assessment of normal flow patterns in the pulmonary circulation by using 4D magnetic resonance velocity mapping. *Magn Reson Imaging* 31:178–188
43. Capuano F, Loke Y-H, Balaras E (2019) Blood flow dynamics at the pulmonary artery bifurcation. *Fluids* 4:190
44. Riesenkampff E, Nordmeyer S, Al-Wakeel N, Kropf S, Kutty S, Berger F, Kuehne T (2014) Flow-sensitive four-dimensional velocity-encoded magnetic resonance imaging reveals abnormal blood flow patterns in the aorta and pulmonary trunk of patients with transposition. *Cardiol Young* 24:47–53
45. Rickers C, Kheradvar A, Sievers HH, Falahatpisheh A, Wegner P, Gabbert D, Jerosch-Herold M, Hart C, Voges I, Putman LM, Kristo I, Fischer G, Scheewe J, Kramer HH (2016) Is the Lecompte technique the last word on transposition of the great arteries repair for all patients? A magnetic resonance imaging study including a spiral technique two decades postoperatively. *Interact Cardiovasc Thorac Surg* 22:817–825
46. Villafañe J, Lantin-Hermoso MR, Bhatt AB, Tweddell JS, Geva T, Nathan M, Elliott MJ, Vetter VL, Paridon SM, Kochilas L (2014) D-transposition of the great arteries: the current era of the arterial switch operation. *J Am Coll Cardiol* 64:498–511
47. Fricke TA, d'Udekem Y, Richardson M, Thuys C, Dronavalli M, Ramsay JM, Wheaton G, Grigg LE, Brizard CP, Konstantinov IE (2012) Outcomes of the arterial switch operation for transposition of the great arteries: 25 years of experience. *Ann Thorac Surg* 94:139–145
48. Vukicevic M, Chiulli JA, Conover T, Pennati G, Hsia TY, Figliola RS (2013) Mock circulatory system of the Fontan circulation to study respiration effects on venous flow behavior. *ASAIO J* 59:253–60
49. Biglino G, Verschuere P, Zegels R, Taylor AM, Schievano S (2013) Rapid prototyping compliant arterial phantoms for in-vitro studies and device testing. *J Cardiovasc Magn Reson* 15:2
50. de Zélicourt DA, Pekkan K, Wills L, Kanter K, Forbess J, Sharma S, Fogel M, Yoganathan AP (2005) In vitro flow analysis of a patient-specific intraatrial total cavopulmonary connection. *Ann Thorac Surg* 79:2094–2102
51. Gehron J, Zirbes J, Bongert M, Schäfer S, Fiebich M, Krombach G, Böning A, Grieshaber P (2019) Development and validation

of a life-sized mock circulatory loop of the human circulation for fluid-mechanical studies. *ASAIO J* 65:788–797

Publisher's Note Springer Nature remains neutral with regard to jurisdictional claims in published maps and institutional affiliations.